J Mater Sci (2008) 43:155–163
DOI 10.1007/s10853-007-2140-6

Splitting behavior and structural transformation process of $K_2Ti_6O_{13}$ whiskers under hydrothermal conditions

Yaxin Zhou · Chang Liu · Ming He · Xiaohua Lu · Xin Feng · Zhuhong Yang

Received: 26 March 2007 / Accepted: 4 September 2007 / Published online: 29 September 2007

Abstract The splitting behavior and structural transformation process of $K_2Ti_6O_{13}$ whiskers in various hydrothermal solutions were investigated by the X-ray diffraction technique, scanning electron microscopy, transmission electron microscopy, and atomic force microscopy. TiO_2 (B) particle aggregates and rutile twinned crystals were produced respectively in diluted and concentrated HCl solutions via "dissolution-precipitation" mechanism, while no changes were observed in deionized water. In contrary to the chemical inertia of $K_2Ti_6O_{13}$ whiskers in KOH solution, trititanate nanowires were synthesized by splitting the bulk $K_2Ti_6O_{13}$ whiskers in NaOH solution. The driving force for the formation of nanowires originated from the intrinsic strain induced by the phase transition from $K_2Ti_6O_{13}$ with a tunnel structure to layered trititanate.

Introduction

In recent years, due to the interesting size- and shape-dependent properties, one-dimensional (1D) forms of titanium oxides and alkaline metal titanates presented by the chemical formula $R_2Ti_nO_{2n+1}$ (R = proton or alkaline metal ion, n = 2–8) have attracted much attention for possible applications such as catalysts [1, 2], gas sensors [3], lithium-ion-battery materials [4–6], and reinforcing agents [7]. One-dimensional titanates can be classified into two categories according to their diameters: titanate whisker (about 1 μm) and titanate nanostructures (<100 nm) including nanowire and nanotube. Therein, trititanate nanowires with large specific surface area have currently found advanced applications as photocatalysts for the decomposition of water [8] and 4-chlorophenol [9], proton conductors [10], and ion-exchange materials [11]. So far, trititanate nanowires have been produced via hydrothermal methods using TiO_2 as reactant [12–15]. But the exact formation mechanism is still a controversial topic debated in contemporary literature. Wu et al. [16] proposed that thick $Na_2Ti_3O_7$ layers grew during alkaline treatment and split further to form nanowires. Du et al. [17] suggested on the basis of high-resolution transmission electron microscopy (HRTEM) observations that the growth of nanowire was initiated by the formation of crystalline nuclei in TiO_2 matrix, and this was the conclusion of another study as well [18]. Mao et al.[19] assumed that lamellar trititanate was formed on the solid-liquid interface, followed by the rolling up of individual trititanate sheet into nanowire. Other researchers argued that the nanowires were derived from nanotubes after Ostwald ripening [20–22].

The basic frameworks of trititanate are built up by three octahedra sharing edges at one level (Fig. 1a). $K_2Ti_6O_{13}$ with a tunnel structure consists of distorted Ti-O octahedra that enclose the potassium ions (as shown in Fig. 1b). The synthesis routes to $K_2Ti_6O_{13}$ from layered titanates involving trititanate by ion-exchange reactions or

Electronic supplementary material The online version of this article (doi:10.1007/s10853-007-2140-6) contains supplementary material, which is available to authorized users.

Y. Zhou · C. Liu · X. Lu (✉) · X. Feng · Z. Yang
State Key Laboratory of Materials-oriented Chemical Engineering, Nanjing University of Technology, Nanjing 210009, P.R. China
e-mail: xhlu@njut.edu.cn

M. He
Information College of Science and Technology, Nanjing Forestry University, Nanjing 210037, P.R. China

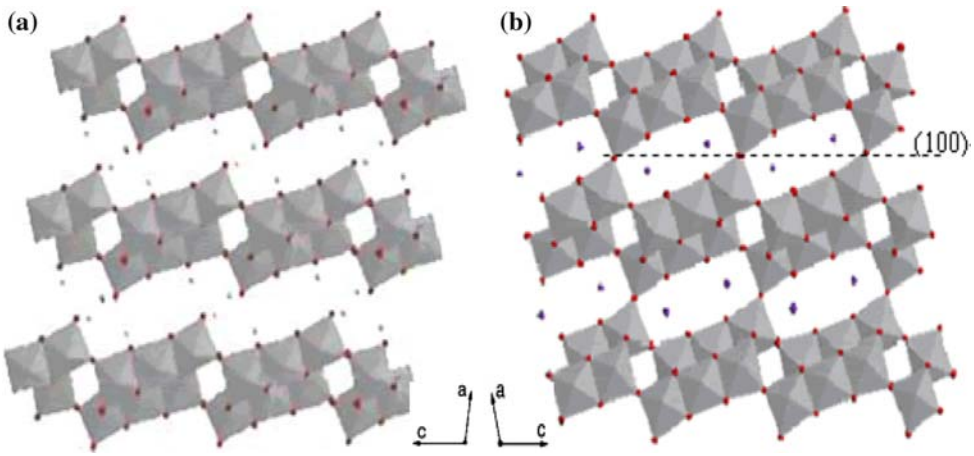

Fig. 1 Crystal structure models of (**a**) Trititanate and (**b**) $K_2Ti_6O_{13}$

calcination methods have been widely studied by many researchers [23–25]. The transition process is understandable and spontaneous due to the difference in the structural stability between them. The strain-induced model was adopted by Wang et al. to explain the formation mechanism [26]. But the feasibility and necessary conditions for the transition from more stable $K_2Ti_6O_{13}$ to layered trititanate have not been investigated yet.

In our previous paper, we found that $K_2Ti_6O_{13}$ whisker (Fig. 2a) is made of lamellas whose diameters are 20–150 nm (Fig. 2b and c) [27]. Endo et al.[28] assumed that there was amorphous K_2O-rich melt in the gaps between $K_2Ti_6O_{13}$ lamellas, and K^+ was slowly stripped from the melt at room temperature [29]. It seems that titanate nanowires can be easily produced by removing the K_2O-rich melt. This potential method may be simpler and more convenient than those referred to above.

In this study, hydrothermal reactions of $K_2Ti_6O_{13}$ whiskers were performed in various aqueous media including acid, neutral, and alkaline solutions. The changes in morphology and structure were studied. This study is favorable for understanding the reversibility of the structural transition between $K_2Ti_6O_{13}$ and trititanate. We would like to emphasize that the contribution of this article is not the synthesis of nanowires, but rather the transformation behaviors of $K_2Ti_6O_{13}$ whiskers under hydrothermal conditions. The transition mechanism will be discussed from the points of view of thermodynamic calculations and crystal-structure changes. Moreover, the microstructure of $K_2Ti_6O_{13}$ whisker was also studied in this work.

Experimental section

Our samples were prepared by hydrothermal methods. $K_2Ti_6O_{13}$ whiskers with an average diameter of 0.6 μm and an average length of 25 μm (Fig. 2a) were prepared through the ion-exchange reaction of layered potassium tetratitanate ($K_2Ti_4O_9$) and a subsequent calcination procedure [30] and were used as the raw material. The whiskers (0.5 g) and 70 mL of solution were placed in a 100-mL Teflon-lined autoclave that was statically heated in a furnace at a heating rate of 5 °C min^{-1} to the specific temperature and kept at the temperature for a certain time as shown in Table 1. The

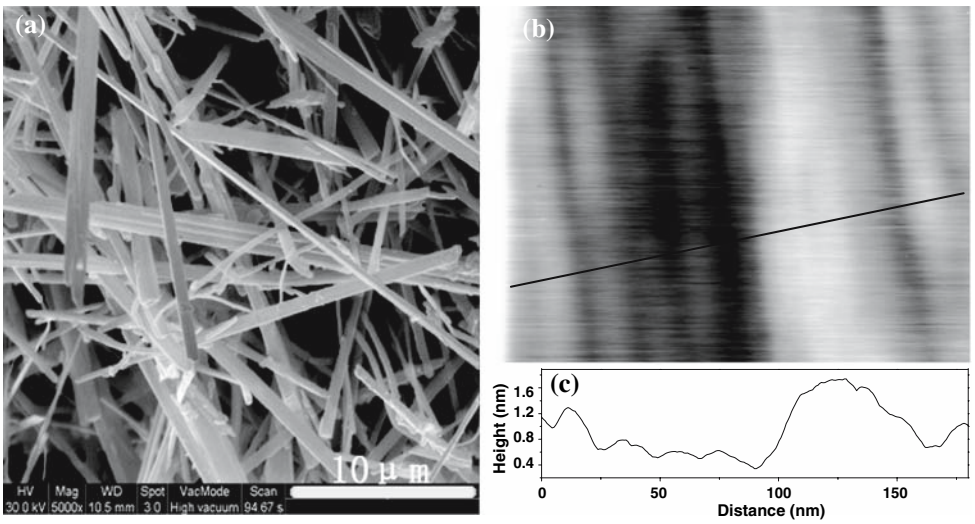

Fig. 2 SEM (**a**) and AFM (200×200 nm^2), (**b**) Images in different magnification scale of $K_2Ti_6O_{13}$ whisker, (**c**) Cross-sectional profile of $K_2Ti_6O_{13}$ whisker in Fig. 2b

Table 1 Solution compositions and reaction conditions

Sample	Solutions	Reaction temperature (°C)	Time (h)
1	HCl (pH = 2)	150	36
2	HCl (pH = 2)	180	12
3	HCl (pH = 0)	150	12
4	Deionized water (pH = 7)	220	36
5	$^{\alpha}$10 mol/Kg NaOH	220	12
6	$^{\alpha}$10 mol/Kg KOH	220	12

Note: α: 10 mol/kg NaOH = $\frac{10 \text{ mol of NaOH}}{1 \text{ kg of } H_2O}$ and 10 mol/Kg KOH = $\frac{10 \text{ mol of KOH}}{1 \text{ kg of } H_2O}$

chemicals were A.R. reagents purchased from Shanghai Chemical Co. and used without further purification. The deionized water (resistivity >15 MΩ cm) was used throughout the experiments. The product was filtered and washed at room temperature with water until pH reached about 7 and then dried at 80 °C in air.

The products were characterized by X-ray diffraction (Bruker D8). CuKα radiation with a nickel filter was used, operating at 40 kV and 30 mA. The powder samples were measured in the continuous scan mode at 5–60°/2θ, with a scanning rate of 0.02°/s. The peak positions and relative intensities were characterized by comparison with International Centre for Diffraction Data (ICDD) standards. The morphology and structure of the products were investigated using a scanning electron microscope (SEM, FEI QUANTA-200), a transmission electron microscope (TEM, JECS-2100) and an atomic force microscope (AFM). The samples used for TEM observation were prepared by dispersing some powder in deionized water followed by mild ultrasonic vibration for half an hour, then dripping a drop of the dispersion onto a copper grid coated with a layer of amorphous carbon. The preparation method for the sample used for AFM imaging was similar to that for TEM characterization, while the sample was dispersed onto the cover glass. AFM (Park Company, Thermomicroscopy Auto Probe Research) was used in air at room temperature. A silicon nitride cantilever with a force constant of 0.26 N/m was used in contact mode. The cantilever was 180-μm long, 25-μm wide and 0.10-μm thick with an attached tip whose apex radius was less than 15 nm. The scan rate was 0.5–3 Hz.

Results and discussion

Hydrothermal reactions of $K_2Ti_6O_{13}$ whiskers in acid and neutral solutions

Although the reaction mechanism of $K_2Ti_4O_9$ in acids is well known [30–34], the transformation behaviors of $K_2Ti_6O_{13}$ in acid solutions were rarely investigated. If the K_2O melt exists in the gaps between $K_2Ti_6O_{13}$ lamellas, the transformation of $K_2Ti_6O_{13}$ whiskers will be more facile in acid solutions. Since Lee et al. [35] reported that titanium was extracted from $K_2Ti_6O_{13}$ at $[H^+] > 0.05$ M (pH = 1.3) at ambient temperature, and the fibrous shape was not destroyed in the process, several treatment conditions, i.e., the concentration of HCl solution, the treatment temperature and time, were attempted. XRD patterns of samples 1, 2, 3, and 4 are presented in Fig. 3. The composition and fibrous shape of the whiskers were not changed after holding the whiskers in pH = 2 HCl solution at 150 °C for 36 h (Figs. 3b and 4a). But the $K_2Ti_6O_{13}$ whiskers began to dissolve into solution and a few precipitated particles attached on the outside of the whiskers. Like a chemical catalyst, acid could accelerate the phase transition and crystal growth. So the transformation process was dramatically accelerated by increasing the reaction temperature or $[H^+]$. The samples 2 and 3 were identified as TiO_2 (B) (Fig. 3c) and rutile (Fig. 3d), respectively. The fibrous shape of sample 2 was destroyed more severely when compared with that of sample 1 and the precipitated particles agglomerated together (Fig. 4b). As seen in Fig. 4c, the micro-size twinned rutile was formed from $K_2Ti_6O_{13}$ whiskers in concentrated HCl solution for the first time. Meanwhile, the fibrous shape disappeared completely. The formation of twinned rutile titania in literature was described only through the complicated hydrolysis/thermolysis of $TiCl_4$ microemulsion [36].

Tournoux et al. [37] and Feist and Davies [34] have presented papers discussing the formation of TiO_2 from such layered titanates as $K_2Ti_4O_9$ and $Na_2Ti_3O_7$. A specific

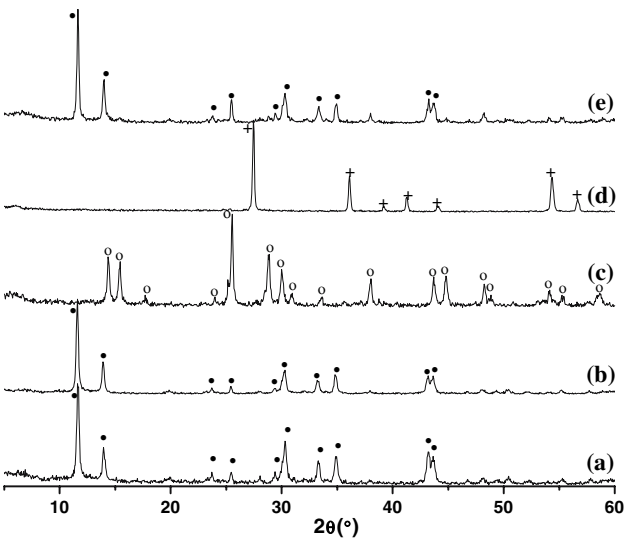

Fig. 3 XRD patterns of raw $K_2Ti_6O_{13}$ whiskers (**a**), Sample 1 (**b**), Sample 2 (**c**), Sample 3 (**d**), and Sample 4 (**e**). (●) $K_2Ti_6O_{13}$, (○) TiO_2 (B), (+) Rutile

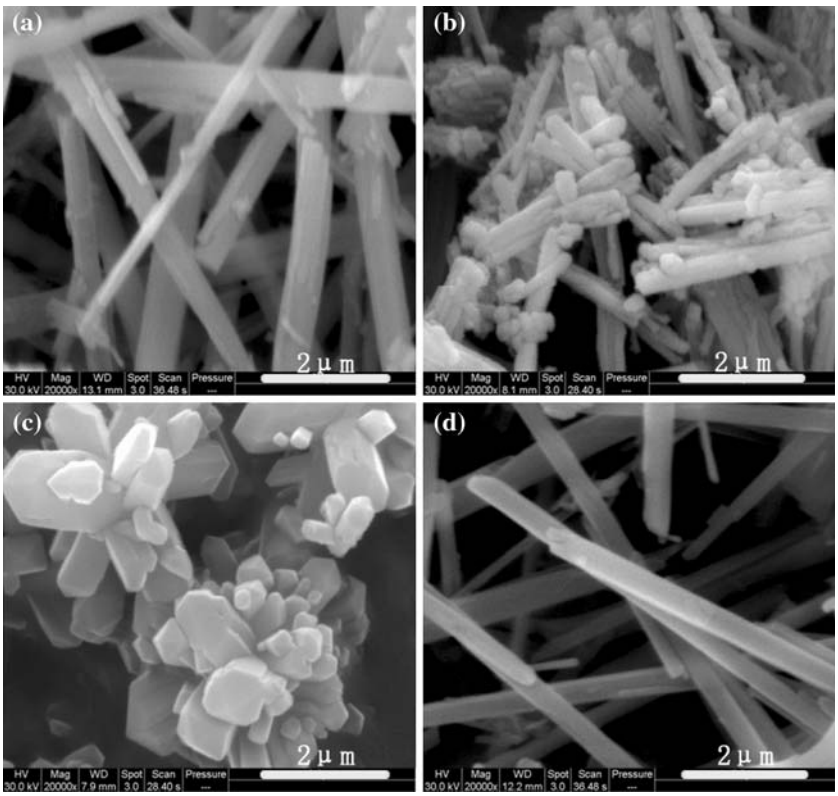

Fig. 4 SEM images of samples treated under different conditions: (**a**) Sample 1 (Fig. 3b), (**b**) Sample 2 (Fig. 3c), (**c**) Sample 3 (Fig. 3d), and (**d**) Sample 4 (Fig. 3e)

mechanism was suggested that the condensation of the layers was followed by a nucleation and growth step to yield TiO_2, but it is not applicable to this study. The transition process of $K_2Ti_6O_{13}$ whiskers in acid solutions can be interpreted by "dissolution-precipitation" model. Two different structural units rearrangement mechanisms based on the effect of the acid concentration were proposed by Zhu et al. to explain the phase transition between hydrogen titanate and titanium dioxides [38]. In this work, the $K_2Ti_6O_{13}$ crystallite was dissolved and shattered to form detached $[TiO_6]$ units, followed by the different reconstructions in diluted and concentrated acid solutions. When the acidity is low, TiO_2 (B) that is composed of corrugated sheets of edge- and corner-sharing TiO_6 octahedra is formed and the crystallites of TiO_2 easily aggregate because of the large surface area. As the acidity is high, TiO_6 octahedra link by sharing an edge to form chains, and then the corner-shared bonding among chains leads to a 3D framework of rutile. The experiment was also performed at 220 °C in deionized water (pH = 7) that was approximate to the infinitely diluted HCl solution. As expected, no changes in composition and morphology were observed (Figs. 3e and 4d). If the K_2O-rich phase exists, it will be easily removed by neutralizing with HCl and then the whiskers can facilely split into nanowires. The conclusions that titanate nanowires cannot be obtained by splitting the $K_2Ti_6O_{13}$ whiskers in neutral or acid solutions and the K_2O-rich phase is non-existent are deduced from above experiments.

Hydrothermal reactions of $K_2Ti_6O_{13}$ whiskers in NaOH and KOH solutions

Although K^+ has similar chemical character to Na^+, it has been noticed that K^+ is not suitable to replace Na^+ in the alkaline reaction because of the irregular morphology of the products [13]. In contemporary literature, trititanate nanostructures were produced via hydrothermal reaction only in NaOH solution [39–41]. To investigate the effect of alkaline environment on the transition of $K_2Ti_6O_{13}$, we performed the reactions in NaOH and KOH solutions, respectively.

Figure 5 shows the XRD patterns of samples 5 and 6. In contrast, the two as-synthesized products had different crystal structures. The peaks for sample 5 can be assigned to trititanate (Fig. 5a) [42]. The average size of the product calculated by Scherrer equation is around 20 nm. We prefer to consider that $Na_2Ti_3O_7$ was obtained before washing [9, 15], while the sodium impurities could be partially removed by treating with water to form a new phase of titanate ($Na_xH_{2-x}Ti_3O_7$) [11]. Further study indicates that only water washing is required to prepare $H_2Ti_3O_7$ ($Na_xH_{2-x}Ti_3O_7$, $x = 0$) that is derived from

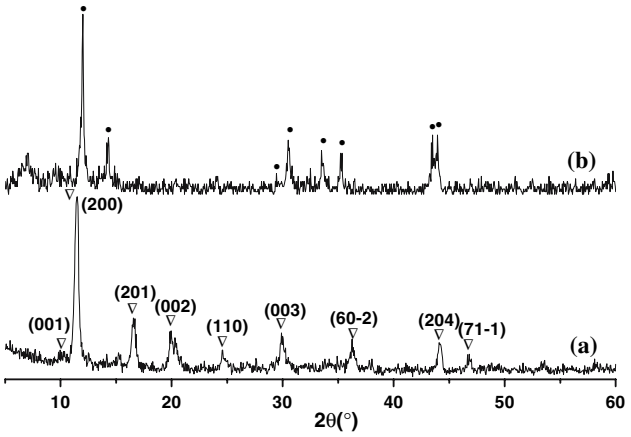

Fig. 5 XRD patterns of (**a**) Sample 5 and (**b**) Sample 6 (▽) trititanate, (●) $K_2Ti_6O_{13}$

$K_2Ti_6O_{13}$ whiskers (Figures S1 and S2 in Supporting Information), and it appears to be a significant improvement over previous reported processes [11, 15, 43]. Only peaks of $K_2Ti_6O_{13}$ appear in the XRD spectrum of sample 6, indicating no phase transition that takes place in KOH solution (Fig. 5b).

The morphology of sample 5 was remarkably different from that of the raw material, that is, nanowires with diameters of 20–30 nm were observed (Fig. 6a and b), and the size is consistent with the result of XRD. The trititanate structure was also characterized by HRTEM (Fig. 6c). The fringes parallel to the longitudinal direction of the wire axis with a ca. 0.79 nm interplanar distance correspond to the structural features of the interlayer spacing of d_{200}, in agreement with the result reported by Lan et al. [21] and the value is slightly larger than that (0.782 nm) derived from XRD reflections [42]. Another set of fringes toward wire periphery with ca. 0.36 nm spacing is assigned to the (110) plane of the trititanate crystal structure. The Fast Fourier transformation (FFT) pattern of the single nanowire indicates the layered structure of trititanate, a conclusion which is consistent with previous report [5]. The difference in morphology between sample 6 and the raw $K_2Ti_6O_{13}$ whiskers could hardly been observed (Fig. 6d).

AFM is an invaluable technique for studying high-resolution 3D topographies of various nanowires. To our knowledge, there were no studies on that of trititanate nanowire in the literature. Figure 7a shows the AFM image (0.5 μm × 0.5 μm Topography) of single trititanate nanowire surface. The diameter of this scanned nanowire is around 50 nm, larger than the average diameter value. Since 3D image in real space can be observed by AFM, the plane index can be obtained directly by measuring the angles between the planes. This method has been used to study the sidewall angle artifact [44] and GaAs epilayer growth [45]. The contour of the line is shown in Fig. 7b. The angles resulted from the theory for (1–13) plane, (200)

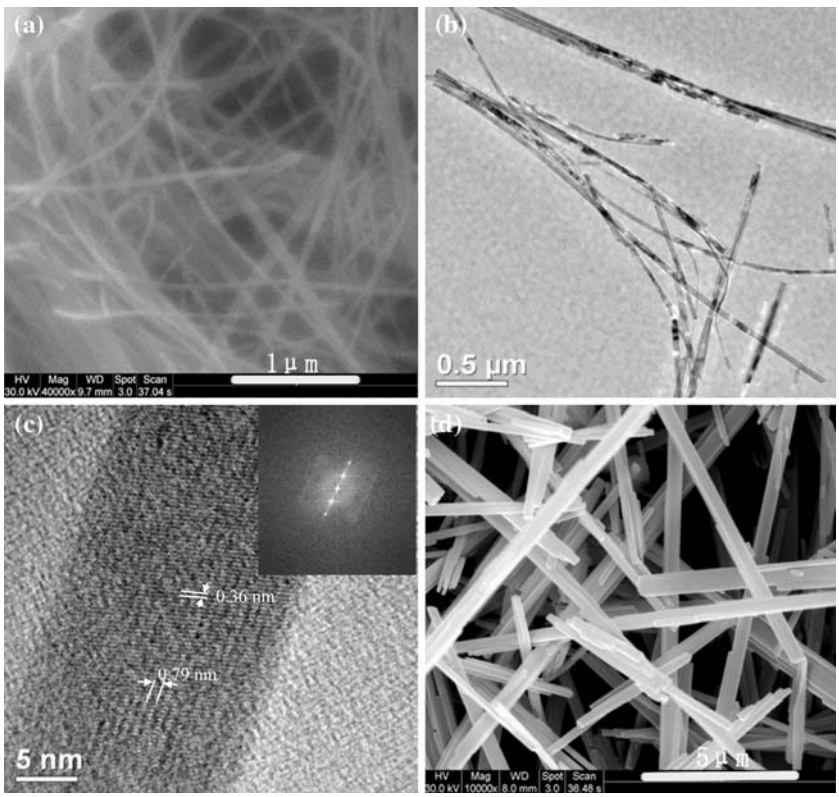

Fig. 6 SEM and TEM images of sample 5 (**a**, **b**, and **c**) and sample 6 (**d**). Inset: FFT pattern of sample 5 (**c**)

plane and (202) plane are 116° and 138°, respectively, coinciding with the experimental data of 117° and 139°. So the indexes of the three planes were determined. The (200) plane observed by XRD and HRTEM is clearly shown here, suggesting it is a main plane of trititanate. In previous studies, the (202) plane was usually detected by electron diffraction [20, 39] and the growth along [101] direction was considered to result in the width of the nanostructures [18]. The (110) plane that was not found here might be in the cross section in Fig. 7b.

Thermodynamic feasibility of the structural transitions of $K_2Ti_6O_{13}$ in NaOH and KOH solutions

Equations for $K_2Ti_6O_{13}$ reacting with NaOH and KOH solutions are respectively expressed by Eqs. 1 and 2, therein KOH(∞H_2O) is the KOH that is infinitely diluted by abundant NaOH solution. Unlike $Na_2Ti_3O_7$, $K_2Ti_3O_7$ is an unstable intermediate phase during the formation of other potassium titanates [46, 47]. It is acknowledged that $K_2Ti_4O_9$ is the stable phase which can be formed from the association reaction between $K_2Ti_6O_{13}$ and K_2O-rich melt [48].

$$K_2Ti_6O_{13} + 4NaOH \longrightarrow 2Na_2Ti_3O_7 + 2KOH(\infty H_2O) + H_2O \quad (1)$$

$$2K_2Ti_6O_{13} + 2KOH \longrightarrow 3K_2Ti_4O_9 + H_2O \quad (2)$$

In this study, the amplitude of the pressure change in autoclave is around 1 MPa, hardly affecting the reactions. To estimate the possibility of the chemical reactions, the Gibbs energy changes in the reactions were calculated under certain conditions to determine the reaction direction. The Gibbs energy change with the change of temperature is expressed by,

$$\Delta G^o_{f,T} = \Delta H^o_{f,298} - T\Delta S^o_{f,298} + \int_{298}^{T} \Delta C_P dT - T\int_{298}^{T} \frac{\Delta C_P}{T} dT$$

$$\Delta S^o_{f,298} = (\Delta H^o_{f,298} - \Delta G^o_{f,298})/298$$

where $\Delta G^o_{f,T}$, $\Delta H^o_{f,T}$, $\Delta S^o_{f,T}$ and ΔC_P are the changes of the Gibbs energy, enthalpy, entropy and heat capacity at temperature T, respectively. In hydrothermal reactions, the quantity of the solvent is much more abundant than solid raw materials, so we consider that the thermodynamic data of KOH(∞H_2O) are approximate to those of H_2O. For ordinary compounds of NaOH solution, KOH solution, H_2O, and $Na_2Ti_3O_7$, the relations between thermodynamic data and temperature can be obtained from handbooks [49, 50]. To obtain the thermodynamic properties of the compounds whose thermodynamic data cannot be got from literatures or handbooks, the model introduced by Bao et al. is used [51]. The data for $Na_2Ti_3O_7$ are compared to proof the accuracy of the model. As seen in Table 2, the estimating method can be applied to alkaline metal titanates. If the Gibbs energy change at T is <0, the reaction will proceed spontaneously. It can be found that neither of the two reactions will take place at room temperature because $\Delta G_{r,298}$ is positive. While $\Delta G_{r,493}$ of reaction (1) at 220 °C is <0, suggesting that reaction (1) is thermodynamically favored. The analysis was proved by the characterization results (Figs. 5a and 6a–c). We calculated the changes in entropy and enthalpy to clarify the further reasons for this reaction. The hydration of K^+ ions diluted into solution can gain the entropy, while both the dehydration of double amount of $Na^+(H_2O)_n$ and the transition from $K_2Ti_6O_{13}$ with a stable tunnel structure to layered $Na_2Ti_3O_7$ promote the entropy loss. So the change in entropy is negative ($\Delta S_{f,493}$ = –1.95 kJ mol^{-1} K^{-1}). But $\Delta H_{f,493}$ (–992.21 kJ mol^{-1}), which results from the phase transition, the dilution of extracted K^+, the dehydration of $Na^+(H_2O)_n$, and the hydration of K^+, is much less than $T\Delta S_{f,493}$ (–961.35 kJ mol^{-1}), showing that this reaction is

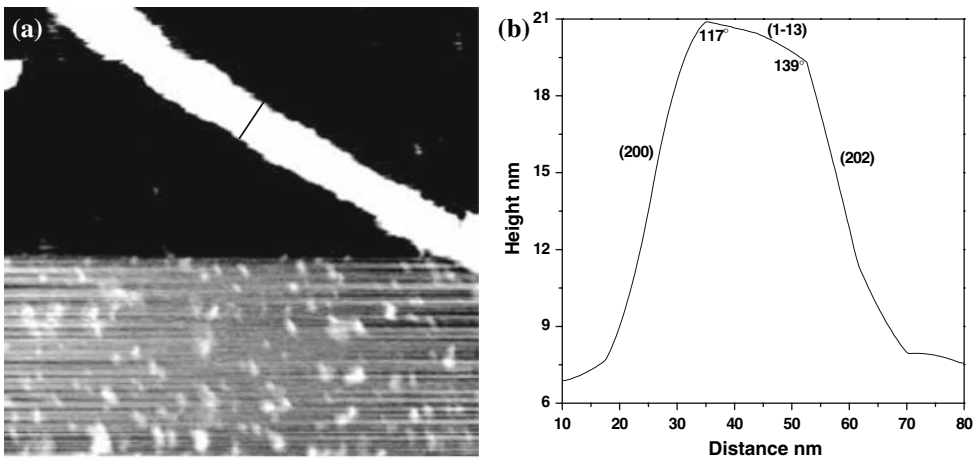

Fig. 7 AFM morphology pictures of sample 5: (**a**) 500 × 500 nm^2 and (**b**) Cross-sectional profile analysis in Fig. 7a

Table 2 Thermodynamic calculations for the reactions

Material	$\Delta G^o_{f,298}$ (kJ mol^{-1})		$\Delta H^o_{f,298}$ (kJ mol^{-1})		C_p (J mol^{-1} K^{-1})			$\Delta G_{r,298}$ (kJ mol^{-1})		$\Delta G_{r,493}$ (kJ mol^{-1})	
	Cited	Calculated	Cited	Calculated	a	b	c	Eq. 1	Eq. 2	Eq. 1	Eq. 2
NaOH (10 mol/kg)$^{\alpha,\beta}$	–379.74		–425.97		4650.99	–15.89	0.022	127.77	65.44	–30.78	190.03
KOH (10 mol/kg)$^{\alpha,\beta}$	–378.86		–424.73		2918.87	–3.96	0.0085				
H_2O, KOH(∞H_2O)$^{\alpha,\beta}$	–228.62		–241.83		28.83	0.014	-1.46×10^{-6}				
$Na_2Ti_3O_7^{\beta,\gamma}$	–3277.43	–3150.60	–3479.96	–3481.46	198.92	0.12	-3.56×10^{-5}				
$K_2Ti_6O_{13}^{\delta}$		–5849.53		–6353.32	80.90	44.91×10^{-3}	-21×10^5				
$K_2Ti_4O_9^{\delta}$		–4054.24		–4479.98	80.47	21.60×10^{-3}	-15×10^5				

Notes: α: Ref. [49]; β: the coefficients for C_p was regressed by equation $C_P = a + bT + cT^2$; γ: Ref. [50]; δ: the coefficients for C_p was estimated by Kubaschewski equation using $C_P = a + bT + cT^{-2}$

dominated by the change in enthalpy rather than the change in entropy. So $\Delta G_{r,493}$ is <0 for reaction (1) and the transition process can proceed. The reaction (2) is thermodynamically disfavored at the same temperature due to $\Delta G_{r,493} > 0$, consistent with the fact that the changes in the composition and morphology of $K_2Ti_6O_{13}$ whiskers could not be observed by XRD and SEM. In addition, the energy barrier for structural transformation from $(Ti_3O_7)^{2-}$ frameworks in $K_2Ti_6O_{13}$ to $(Ti_4O_9)^{2-}$ layers in $K_2Ti_4O_9$ is so high that the calcination process is usually needed [52].

The effect of different base on the structural and morphological transformations of $K_2Ti_6O_{13}$ whiskers

Although $K_2Ti_6O_{13}$ bears high chemical stability in air, the binding between adjacent $(Ti_3O_7)^{2-}$ frameworks is weak. The weakest binding plane in $K_2Ti_6O_{13}$ is (100) [53]. The reaction temperature chosen in Ref. [26] was lower than that in this work, indicating that the splitting process of $K_2Ti_6O_{13}$ needs more energy than the formation process. Besides KOH, other alkaline solutions such as LiOH, $Ba(OH)_2$ and $Ca(OH)_2$ were used as hydrothermal solvents, but only particles were obtained. Furthermore, when NaOH solution was replaced by NaCl or KCl solution, no changes were observed. The alkali-metal cations interaction with water may be the crucial factor for the splitting process. The hydration number of ions will reduce sharply in a concentrated solution when compared with that in a diluted solution, which results in needing lower energy for dehydration. In addition, the dehydration energies for $Na^+(H_2O)_n$ are higher than those for $K^+(H_2O)_n$ [54], which indicates that Na^+ ions with stronger solvating ability have more amount of OH^- around them than that around K^+ ions. So the concentrated Na^+ and OH^- co-exist environment is essential for the synthesis of the trititanate nanowires. The plausible model for the transformation from $K_2Ti_6O_{13}$ whiskers to trititanate nanowires is proposed: In bulk NaOH solution, the outside of $K_2Ti_6O_{13}$ was taken up by $Na^+(H_2O)_n$ and the bonded OH^-. The two sides of $(Ti_3O_7)^{2-}$ on the top surface were in different chemical environments, and the different charge field between two sides induced the surface tension that had a tendency to split along (100) plane (Fig. 1b). $Na^+(H_2O)_n$ was dehydrated and Na^+ ions, which are smaller than K^+, were intercalated into the interlayers and the replacement process resulted in the intrinsic strain. Then the layers shifted about 1/2 b along the [010] direction and a small amount along the [001] direction to form trititanate. The rod axis of $K_2Ti_6O_{13}$ or $Na_2Ti_3O_7$ was along the [010] direction [26, 53], and the lattice mismatch among the (100) type atomic planes of $K_2Ti_6O_{13}$ and $Na_2Ti_3O_7$ was only 8.9% [26]. So this might be an opposite transition process to that described by Wang et al. [26]. Since the Na^+ ions were weakly bonded to the negatively charged Ti_3O_7 layers, the Ti–O–Na^+ bond was converted into Ti–O–H^+ bond when the sample was treated with water.

The material in nano-gaps between $K_2Ti_6O_{13}$ lamellas is the individual or aggregated thinner fibrous $K_2Ti_6O_{13}$ in lower position and cannot be detected by AFM tip (Scheme 1a). The whisker was split due to the strain in the cohesive sections when the tunnel structure was converted into layered structure. First, the thinner whiskers in lower position are more easily separated from the bulk and the lamellas are also exfoliated at the same time (Fig. 8a, Scheme 1b). Then, the increasing strain results in the further split of lamellas to form nanowires (Fig. 8b, Scheme 1c).

In KOH solution, the difference charge field, which is caused by K^+ in the lattice and $K^+(H_2O)_n$ with less amount of OH^- on the top surface, is too small to make $K_2Ti_6O_{13}$ split along (100) plane, so the reaction cannot take place.

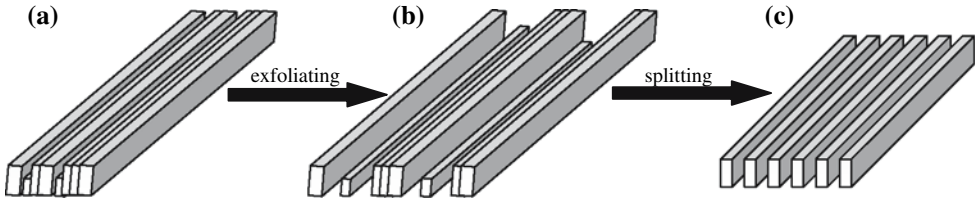

Scheme 1 Schematic drawings depicting the formation process of nanowires: (**a**) $K_2Ti_6O_{13}$ whiskers constituted of lamellar structures and the thinner whiskers in lower position, (**b**) Exfoliation of the lamellas and thinner whiskers, (**c**) Nanowires formed by further split

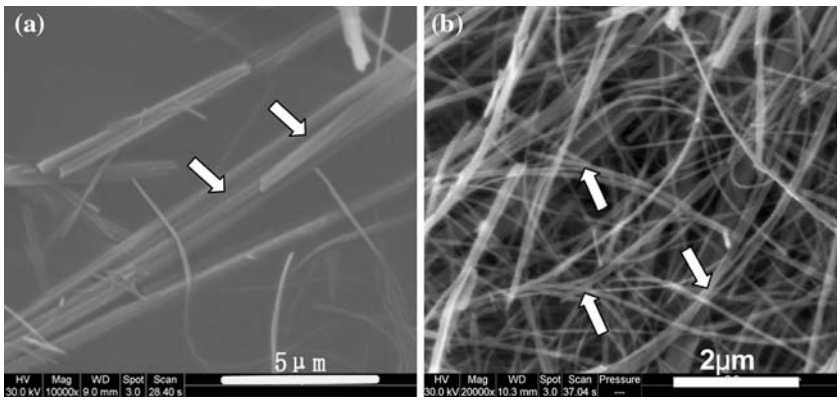

Fig. 8 Morphology evolution in the formation of nanowires: (**a**) A crack developing in the whisker and (**b**) Further split to form nanowires that were indicated by arrows

Conclusion

The splitting behavior and structural transformation process of $K_2Ti_6O_{13}$ whiskers in various hydrothermal solutions were studied. TiO_2 (B) particle aggregates and rutile twinned crystals were obtained respectively in diluted and concentrated HCl solutions via "dissolution-precipitation" mechanism. In contrary to the chemical inertia of $K_2Ti_6O_{13}$ whiskers in deionized water and in KOH solution, the layered trititanate was produced in NaOH solution, accompanying the sequence of exfoliation and split of $K_2Ti_6O_{13}$ lamellas to form nanowires. It was deduced that the concentrated Na^+ and OH^- co-exist environment was essential for the synthesis of trititanate nanowires. The significance of this work is: because of the giant strain, it is difficult to synthesize the titanate nanowires from bulk whiskers and maintain the crystal structure at the same time. We also demonstrated that there was no K_2O-rich melt but thin whiskers in gaps between $K_2Ti_6O_{13}$ lamellas. This structural model of $K_2Ti_6O_{13}$ whisker can explain the experimental findings well.

Acknowledgements The authors appreciate Chinese National Science Foundation for Outstanding (No.29925616 and 20428606), Chinese National Natural Foundation (No. 20236010, 20246002 and 20376032), Natural Foundation of Jiangsu Province (BK2004215), Chinese National High-tech Research Development Program (863 Program: 2003AA333010 and 2006AA03Z455), Chinese National Fundamental Research Development Program (973 Program: 2003CB615700).

References

1. Zhu HY, Gao XP, Lan Y, Song DY, Xi YX, Zhao JC (2004) J Am Chem Soc 126:8380
2. Bao NZ, Feng X, Yang ZH, Shen LM, Lu XH (2004) Environ Sci Technol 38:2729
3. Ramirez-Salgado J, Djurado E, Fabry P (2004) J Eur Ceram Soc 24:2477
4. Li JR, Tang ZL, Zhang ZT (2006) Chem Phys Lett 418:506
5. Li JR, Tang ZL, Zhang ZT (2005) Chem Mat 17:5848
6. Wang BL, Chen Q, Hu J, Li H, Hu YF, Peng LM (2005) Chem Phys Lett 406:95
7. Tjong SC, Meng YZ (1998) Polymer 39:5461
8. Yanagisawa M, Uchida S, Sato T (2000) Int J Inorg Mater 2:339
9. Stengl V, Bakardjieva S, Subrt J, Vecernikova E, Szatmary L, Klementova M, Balek V (2006) Appl Catal B Environ 63:20
10. Corcoran DJD, Tunstall DP, Irvine JTS (2000) Solid State Ion 136:297
11. Sun XM, Li YD (2003) Chem Eur J 9:2229
12. Kasuga T, Hiramatsu M, Hoson A, Sekino T, Niihara K (1998) Langmuir 14:3160
13. Chen Q, Zhou WZ, Du GH, Peng LM (2002) Adv Mater 14:1208
14. Meng XD, Wang DZ, Liu JH, Zhang SY (2004) Mater Res Bull 39:2163
15. Yu HG, Yu JG, Cheng B, Zhou MH (2006) J Solid State Chem 179:349
16. Wu D, Liu J, Zhao XN, Li AD, Chen YF, Ming NB (2006) Chem Mat 18:547
17. Du GH, Chen Q, Han PD, Yu Y, Peng LM (2003) Phys Rev B 67:035323
18. Yuan ZY, Colomer JF, Su BL (2002) Chem Phys Lett 363:362
19. Mao YB, Kanungo M, Hemraj-Benny T, Wong SS (2006) J Phys Chem B 110:702
20. Ma RZ, Fukuda K, Sasaki T, Osada M, Bando Y (2005) J Phys Chem B 109:6210

21. Lan Y, Gao XP, Zhu HY, Zheng ZF, Yan TY, Wu F, Ringer SP, Song DY (2005) Adv Funct Mater 15:1310
22. Mao YB, Wong SS (2006) J Am Chem Soc 128:8217
23. Izawa H, Kikkawa S, Koizumi M (1982) J Phys Chem 86:5023
24. Sasaki T, Watanabe M, Fujiki Y, Kitami Y (1994) Chem Mat 6:1749
25. Wang BL, Chen Q, Wang RH, Peng LM (2003) Chem Phys Lett 376:726
26. Wang RH, Chen Q, Wang BL, Zhang S, Peng LM (2005) Appl Phys Lett 86:133101
27. Xie JW, Lu XH, Zhu Y, Liu C, Bao NZ, Feng X (2003) J Mater Sci 38:3641
28. Endo T, Nagayama H, Sato T, Shimada M (1988) J Mater Sci 23:694
29. Harada H, Kudoh Y, Inoue Y, Shima H (1995) J Ceram Soc Jpn 103:155
30. Bao NZ, Lu XH, Ji XY, Feng X, Xie JW (2002) Fluid Phase Equilib 193:229
31. Yin S, Uchida S, Fujishiro Y, Aki M, Sato T (1999) J Mater Chem 9:1191
32. Yin S, Sato T (2000) Ind Eng Chem Res 39:4526
33. Sasaki T, Watanabe M, Komatsu Y, Fujiki Y (1985) Inorg Chem 24:2265
34. Feist TP, Davies PK (1992) J Solid State Chem 101:275
35. Lee CT, Um MH, Kumazawa H (2000) J Am Ceram Soc 83:1098
36. Li GL, Wang GH, Hong JM (1999) J Mater Sci Lett 18:1243
37. Tournoux M, Marchand R, Brohan L (1986) Prog Solid State Chem 17:33
38. Zhu HY, Lan Y, Gao XP, Ringer SP, Zheng ZF, Song DY, Zhao JC (2005) J Am Chem Soc 127:6730
39. Kasuga T, Hiramatsu M, Hoson A, Sekino T, Niihara K (1999) Adv Mater 11:1307
40. Zhang S, Peng LM, Chen Q, Du GH, Dawson G, Zhou WZ (2003) Phys Rev Lett 91:256103
41. Kukovecz A, Hodos N, Horvath E, Radnoczi G, Konya Z, Kiricsi I (2005) J Phys Chem B 109:17781
42. Thorne A, Kruth A, Tunstall D, Irvine JTS, Zhou WZ (2005) J Phys Chem B 109:5439
43. Poudel B, Wang WZ, Dames C, Huang JY, Kunwar S, Wang DZ, Banerjee D, Chen G, Ren ZF (2005) Nanotechnology 16:1935
44. Dixson RG, Sullivan NT, Schneir J, McWaid TH, Tsai VW, Prochazka JJ, Young M (1996) Proc SPIE 2725:572
45. Umeno A, Bacchin G, Nishinaga T (2000) J Cryst Growth 220:355
46. Liu C, He M, Lu XH, Zhang QT, Xu ZZ (2005) Cryst Growth Des 5:1399
47. Liu C, Lu XH, Yu G, Feng X, Zhang QT, Xu ZZ (2005) Mater Chem Phys 94:401
48. Choy JH, Han YS (1998) Mater Lett 34:111
49. Zaytsev IO, Aseyev GG (2000) In: Properties of auqeous solutions of electrolytes. CRC Press Inc., Boca Raton, Florida, p 356
50. Barin I (2003) In: Thermochemical data of pure substances. WILEY-VCH Verlag GmbH, Weinheim, Germany, p 1144
51. Bao NZ, Feng X, Lu XH, Shen LM, Yanagisawa K (2004) AIChE J 50:1568
52. Zaremba T, Hadrys A (2004) J Mater Sci 39:4561
53. Li GL, Liu M, Wang GH (2001) J Mater Res 16:3614
54. Dzidic I, Kebarle P (1970) J Phys Chem 74:1466